HAL
open science

Crystal, electronic and magnetic structures of a novel series of intergrowth carbometalates R4Co2C3 (R = Y, Gd, Tb)

Volodymyr Levytskyi, Olivier Isnard, Reinhard K. Kremer, Volodymyr Babizhetskyy, Bruno Fontaine, Xavier Rocquefelte, Jean-François Halet, Roman Gumeniuk

To cite this version:

Volodymyr Levytskyi, Olivier Isnard, Reinhard K. Kremer, Volodymyr Babizhetskyy, Bruno Fontaine, et al.. Crystal, electronic and magnetic structures of a novel series of intergrowth carbometalates R4Co2C3 (R = Y, Gd, Tb). Dalton Transactions, 2021, 50 (12), pp.4202-4209. 10.1039/d1dt00420d . hal-03217047

HAL Id: hal-03217047

https://hal.science/hal-03217047

Submitted on 15 Jun 2021

HAL is a multi-disciplinary open access archive for the deposit and dissemination of scientific research documents, whether they are published or not. The documents may come from teaching and research institutions in France or abroad, or from public or private research centers.

L'archive ouverte pluridisciplinaire **HAL**, est destinée au dépôt et à la diffusion de documents scientifiques de niveau recherche, publiés ou non, émanant des établissements d'enseignement et de recherche français ou étrangers, des laboratoires publics ou privés.

ARTICLE

Crystal, electronic and magnetic structures of a novel series of intergrowth carbometalates $R_4Co_2C_3$ (R = Y, Gd, Tb)

Volodymyr Levytskyi, [a] Olivier Isnard, [b] Reinhard K. Kremer, [c] Volodymyr Babizhetskyy, [d] Bruno Fontaine, [e] Xavier Rocquefelte, [e] Jean-François Halet[e,f] and Roman Gumeniuk*[a]

A series of new ternary isostructural $R_4Co_2C_3$ (R = Y, Gd, Tb) carbides was synthesized by annealing of arc-melted stoichiometric samples. The crystal structure of $Tb_4Co_2C_3$ [space group $P2/m$, Pearson symbol $mP18$, a = 12.754(2) Å, b = 3.6251(4) Å, c = 7.0731(9) Å, β = 105.601(6)°] was solved by direct methods from neutron powder diffraction data collected at 100 K. The room temperature unit cell parameters of the new phases were determined by X-ray powder diffraction technique. The crystal structure of $Tb_4Co_2C_3$ is characterized as an intergrowth structure resulting from the stacking of alternating TbCoC (YCoC-type) and Tb_2C (anti-$CdCl_2$ type) fragments with a 2:1 ratio. $Tb_4Co_2C_3$ orders ferromagnetically at T_C = 35(1) K, whereas the isostructural $Gd_4Co_2C_3$ reveals two magnetic transitions at T_{C1} = 82(3) K and T_{C2} = 13(2) K. Density functional theory (DFT) calculations confirm that the magnetic moments of the $R_4Co_2C_3$ (R = Gd, Tb) carbides are exclusively due to the rare-earth elements. $Y_4Co_2C_3$ is shown to be a Pauli-paramagnet by experimental and theoretical studies.

Accepted manuscript

Introduction

Carbides reveal a number of fascinating chemical and physical properties and thus, have found their application in industry and daily life. The most prominent examples are WC, carborundum (SiC), TiC or B_4C which are used as cutting tools, in high-powered semiconductor devices, to obtain highly porous carbon materials and as extremely hard refractory material, respectively.[1–3] From the chemical point of view, binary carbides can be considered as ionic (*e.g.* LaC_2, CaC_2, Al_4C_3 *etc.*), covalent (SiC, B_4C) or metallic (TiC, ZrC) compounds.[4] However, this simple classification fails in the description of ternary or higher carbides, where a combination of the above mentioned bonding types frequently occurs. Therefore, ternary carbides with composition $R_xT_yC_z$ (R = rare-earth or actinides, T = transition metal) have been classified as metal-rich carbides [*i.e.*, $(x + y)/z \geq 4$] (*e.g.* $R_2T_{17}C_{3-x}$, $RT_{11}C_{2-x}$, $R_2T_{22}C_{2-x}$, $R_{11}T_{60}C_6$, $R_2T_{14}C_x$) or carbometalates [*i.e.*, $(x + y)/z \leq 2$] (*i.e.*, stoichiometric carbides containing covalently bound $[T_yC_z]^{n-}$ complex anionic sublattice).[5,6]

In crystal structures of carbides with high metal content the isolated C^{4-} ligands are usually incorporated into the octahedral or trigonal prismatic voids and can also occupy partially their crystallographic sites, which frequently results in the formation of a homogeneity range.[7–9] Such a situation is met in about 20 of the 60 known structure types, while others are characterized by the appearance of $[C_2]^{m-}$ and/or $[C_3]^{n-}$ entities.[10] In a classical approach the charge-balance formulae of carbometalates is given as $R^{m+}{}_x[T_yC_z]^{xm-}$. With rare-earths or actinides here expected as R^{3+} cations and isolated C^{4-} – or $[C_2]^{4-}$ entities (with double-bonded carbon atoms) – one could expect the central atoms T of the complex anion $[T_yC_z]^{n-}$ to adopt zero or a slightly positive oxidation state. However, the situation becomes much more complex if a combination of C^{4-}, $[C_2]^{m-}$ and/or $[C_3]^{n-}$ moieties occurs in a structure. This is the case in *e.g.*, $R_4Ni_2C_5$[11], $R_{12}Mn_5C_{15}$[12] and $R_5Re_2C_7$.[13]

Recently, the new Tb_2CoC_2 carbometalate fulfilling the condition $(x + y)/z \leq 2$ was reported.[6,14] However, its crystal structure was determined by X-ray powder diffraction only, which did not allow to precisely localize the light C atoms. In the present work we re-investigated the crystal structure of this compound by means of neutron powder diffraction technique. We find a slightly lower carbon content, *i.e.*, the composition $Tb_4Co_2C_3$ with a monoclinic crystal structure. Other $R_4Co_2C_3$ (R = Y, Gd) phases were shown to crystallize with this unique structure type, which can be considered as an

[a.] *Institut für Experimentelle Physik, TU Bergakademie Freiberg, Leipziger Str. 23, 09596 Freiberg, Germany.*
[b.] *Institut Néel, University Grenoble Alpes and CNRS, 25 rue des martyrs, BP 166, F-38042 Grenoble cedex 9, France.*
[c.] *Max Planck Institute for Solid State Research, Heisenbergstr. 1, D-70569 Stuttgart, Germany.*
[d.] *Department of Inorganic Chemistry, Ivan Franko National University of Lviv, Kyryla i Mefodiya Str. 6, UA-79005 Lviv, Ukraine.*
[e.] *Univ. Rennes, Ecole Nationale Supérieure de Chimie de Rennes, CNRS, Institut des Sciences Chimiques de Rennes-UMR 6226, F-35000 Rennes, France.*
[f.] *CNRS-Saint Gobain-NIMS, IRL 3629, Laboratory for Innovative Key Materials and Structures (LINK), National Institute for Materials Science (NIMS), Tsukuba, 305-0044, Japan.*
† ORCIDs: Volodymyr Levytskyi 0000-0003-0874-8833; Reinhard K. Kremer 0000-0001-9062-2361; Volodymyr Babizhetskyy 0000-0002-0267-0206; Xavier Rocquefelte 0000-0003-0191-2354; Jean-François Halet 0000-0002-2315-4200; Roman Gumeniuk 0000-0002-5003-620X.
Electronic Supplementary Information (ESI) available. See DOI: 10.1039/x0xx00000x

intergrowth of fragments of YCoC and anti-$CdCl_2$ types. The results of our investigation on the synthesis and crystal structure of these novel compounds $R_4Co_2C_3$ (R = Y, Gd) as well as their magnetic properties and electronic structures are reported here.

Experimental

A series of samples with different stoichiometries around the composition "$R_5Co_2C_4$" [nominal composition used for Tb_2CoC_2 synthesis by Levytskyy *et al.*, 2016[14]] (R = rare-earth metals) was prepared by arc melting ingots of yttrium (Chempur, 99.9 wt. %), gadolinium (Strem Chemicals, 99.9 wt. %), and terbium (Sigma Aldrich), cobalt (Chempur, 99.95 wt. %) and graphite pieces (Chempur, 99.9995 wt. %). Heat treatment was performed by annealing the as-cast buttons enclosed in evacuated silica tubes at 800 °C for 2 months followed by rapid quenching in water without breaking the ampoules. The new phases were determined with the ~ 4:2:3 stoichiometry. To perform neutron powder diffraction (NPD) experiments a series of 5 batches with the same $Tb_4Co_2C_3$ composition and a mass of 1 g each were prepared as described above, powdered and mixed together (*i.e.*, total mass of ~5 g).

All synthesized specimens were characterized by powder X-ray diffraction (XRD) using DRON-2.0M (Fe K_α radiation), Philips X'Pert-MPD and Bruker D8 Endeavour (Cu K_α radiation) diffractometers. Phase analysis and refinement of the lattice parameters were performed with the program packages STOE WinXPOW[15] and WinCSD.[16] Blind indexing of the powder XRD patterns of $Tb_4Co_2C_3$ as well as assignment of the space group were performed with the EXPO-2014 program.[17]

NPD patterns of $Tb_4Co_2C_3$ were collected at 100 K at the high flux powder diffractometer D1B installed at the Institut Laue Langevin (ILL, Grenoble, France),[18] operated by the CNRS. Neutrons with the wavelength of 1.28 Å were selected by a focusing germanium (311) monochromator. The polycrystalline sample was loaded into a thin-walled vanadium cylinder of 6 mm in diameter. The structural model of $Tb_4Co_2C_3$ was obtained by direct methods procedure implemented in the WinCSD program package. The final refinement of the structure parameters was performed with the FullProf program package.[19,20]

Measurements of the magnetic susceptibilities were performed in the fields of 0.1, 1.0, 4.0, and 7.0 T and in the temperature range 1.85–300 K with a magnetic property measurement system (Quantum Design, MPMS). Field dependent isothermal magnetization curves were recorded at different temperatures in the field range up to 10 T using the extraction method in a homemade experimental set up that has been described elsewhere.[21] Specific heat capacity was measured in a commercial system PPMS (Quantum Design).

Spin-polarized density functional theory (DFT) calculations were performed on $R_4Co_2C_3$ (R = Y, Gd, Tb) compounds, using the experimental lattice parameters and atomic positions given in Tables 1 and S1†. The calculations were carried out using the full-potential linearized augmented plane wave (FLAPW) approach, as implemented in the WIEN2K code.[22,23] The Perdew, Burke and Ernzerhof (PBE) functional[24] and a plane wave cut-off corresponding to $R_{MT}K_{max}$ = 7 were used. The radial wave functions inside the non-overlapping muffin-tin spheres were expanded up to l_{max} = 12. The charge density was Fourier expanded up to G_{max} = 12 Å^{-1}. The muffin-tin radii were set to 2.36, 2.50, 2.50, 1.88 and 1.47 a.u. for the Y, Gd, Tb, Co and C atoms, respectively. Total energy convergence was achieved with a Brillouin Zone (BZ) integration mesh of 500 k-points, generating 56 k-points in the irreducible part of the Brillouin zone (BZ). All electronic densities of states (DOS) have been plotted considering the Fermi level as the energy reference. To properly treat the localized 4f states of the rare earth elements, the PBE0 hybrid functional[25] was used and the spin-orbit coupling (PBE0+SO) was included,[26] with a magnetization confined along the [010] direction for $Gd_4Co_2C_3$ and $Tb_4Co_2C_3$.

Results and discussion

Crystal structure

Main peaks in the powder X-ray diffraction (PXRD) pattern of $Tb_4Co_2C_3$ sample could be indexed with the monoclinic [space group (SG) $P2/m$] unit cell parameters (UCP) a_0 = 3.5485(3) Å, b_0 = 3.6395(3) Å, c_0 = 12.349(1) Å, β_0 = 90.42(1)° close to those reported earlier.[6,14] Further Rietveld refinement was performed assuming the structure model proposed by Levytskyy *et al.*[14] However, despite it converged with the relatively low reliability factors (*i.e.*, R_I = 2.50 %, R_P = 5.83 %), some theoretically calculated intensities were strongly underestimated as well as few weak reflections seemed to be excluded from the refinement (Fig. 1b). This prompted us to re-index the PXRD pattern of the $Tb_4Co_2C_3$ compound. The new UCPs were found to be related with the old ones as the following: $a \approx \sqrt{(a_0^2 + c_0^2)}$ = 12.8149(6) Å, $b \approx b_0$ = 3.6425(2) Å, $c \approx 2a_0$ = 7.1023(3) Å, whereas β = 105.601(1)°. The analysis of the extinction conditions indicated three possible SGs, *i.e.*, $P2$, Pm and $P2/m$. In the next step, the centrosymmetric SG $P2/m$ was chosen for structural model determination by direct methods. Further Rietveld refinement of the obtained model converged with reliability factors R_I = 2.37 %, R_P = 3.93 %, which were comparable with the given above. Although some additional weak peaks in the PXRD pattern of $Tb_4Co_2C_3$ could be described and the theoretical intensities are now better matching with the experimental profile (Fig. 1c), the atomic coordinates and displacement parameters of carbon atoms could not be refined. Therefore, to solve the crystal structure of the new carbide correctly, neutron powder diffraction measurements at 100 K (to reduce thermal motion of atoms) were performed. The refinement confirmed the correctness of the structure model obtained from the PXRD investigation. The final refined and difference profiles are presented in Fig. 1a (main characteristic range) and Fig. S1 (full pattern), and crystallographic details of the refinement and atomic coordinates are listed in Tables 1 and S1†, respectively. Furthermore, we prepared and found $Y_4Co_2C_3$ and $Gd_4Co_2C_3$ to

Accepted manuscript

be isostructural with the $Tb_4Co_2C_3$ prototype (Fig. S2†, S3† and Tables 1, S1†).

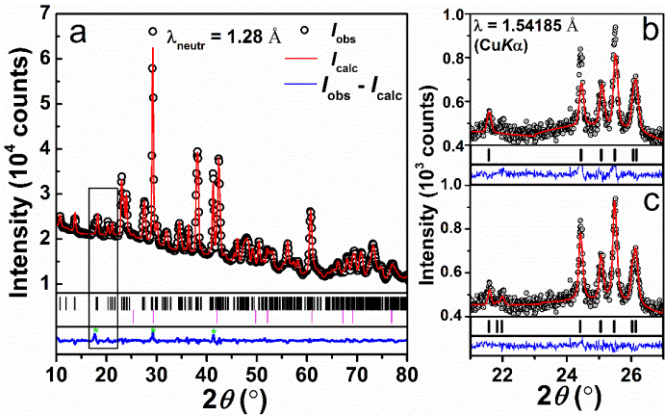

Fig. 1 a) Neutron powder diffraction pattern of $Tb_4Co_2C_3$ collected at 100 K and λ = 1.28 Å. Magenta ticks indicate the positions of Bragg reflections of the *β*-Tb_2C impurity phase (~8.5 wt. %, NaCl structure type, SG $Fm\bar{3}m$, *a* = 5.0406(9) Å, R_B = 3.65 %). b) Selected 2*ϑ*-range of the refined PXRD pattern of $Tb_4Co_2C_3$ assuming a structural model reported earlier[14] (see text for more details). c) Refinement of the PXRD pattern assuming the structural model presented in Tables 1 and 1S†.

Table 1 Details on diffraction data collection and refinement of the $R_4Co_2C_3$ samples (*R* = Y, Gd, Tb)

Temperature	293(2) K	293(2) K	293(2) K	100(1) K
Amount of $R_4Co_2C_3$ phase, *w* (wt. %)*	$Y_4Co_2C_3$ 54(1)[i]	$Gd_4Co_2C_3$ 94(1)[ii]	$Tb_4Co_2C_3$ 97(1)[iii]	$Tb_4Co_2C_3$ 91(2)[iv]
Structure type	$Tb_4Co_2C_3$			
SG (No)	*P2/m* (10)			
Pearson symbol and *Z*	*mP*18, 2			
UCPs				
a, Å	12.859(2)	12.9087(9)	12.8149(6)	12.754(2)
b, Å	3.6404(5)	3.6592(4)	3.6425(2)	3.6251(4)
c, Å	7.0330(8)	7.1797(5)	7.1023(3)	7.0731(9)
β, °	105.32(1)	105.803(4)	105.667(2)	105.601(6)
V, Å³	317.5(5)	326.32(8)	319.20(5)	314.98(7)
Calculated density, g·cm⁻³	5.3(1)	8.0(3)	8.2(1)	8.3(1)
Radiation, *λ* (Å)	Cu K_α, 1.54185			neutrons, 1.28
Mode of refinement	Full profile with constraints and restraints‡			Rietveld
2*ϑ* max, $(sin\vartheta/\lambda)_{max}$	100; 0.49	110, 0.53		127, 0.7
Number of reflections	438	493	487	1199
Number of free parameters	3	3	19	47
Goodness-of-fit, *S*	1.01			2.34
$R_{B(I)}$, in %	9.8	6.6	2.4	3.8
R_p, R_{wp}, in %	8.6, 12.3	3.5; 5.2	3.9; 5.4	7.5; 8.1

* obtained from the full profile refinements; $Y_4Co_2C_3$ as well as R_2C are air sensitive and continuously decomposed even in the paraffin oil during XRD data collection (~ 6.5 h); their amounts could not be determined properly.

[i] Impurity phases included into the refinement: YCoC [*a* = 3.6493(5) Å, *c* = 6.8643(9)Å; R_I = 4.2 %; *w* = 43(2) wt.%] and *β*-Y_2C [*a* = 5.096(1) Å; R_I = 36.9 %; *w* = 4(2) wt.%].

[ii] Impurity phase included into the refinement: *β*-Gd_2C [*a* = 5.046(1) Å; R_I = 41.6 %; *w* = 6(1) wt.%].

[iii] Impurity phase included into the refinement: *β*-Tb_2C [*a* = 5.031(1) Å; R_I = 34.2 %; *w* = 3(1) wt.%].

[iv] Impurity phase included into the refinement: *β*-Tb_2C [refined composition $TbC_{0.71(5)}$; *a* = 5.0406(9) Å, R_B = 3.7 %; *w* = 8.8(7) wt.%].

‡ Atomic coordinates for $Y_4Co_2C_3$ and $Gd_4Co_2C_3$ were constrained to those refined from NPD at 100 K for the $Tb_4Co_2C_3$ structure type. Two final cycles of the least-square refinement of atomic coordinates for $Tb_4Co_2C_3$ were performed with a damping factor.

Interatomic distances of $Tb_4Co_2C_3$ listed in Table S2† were calculated using the unit cell parameters obtained from PXRD at 293 K (Fig. S4†) and the atomic coordinates obtained from the refinement of the NPD data collected at 100 K. As one can see from Table S2†, these values are mainly smaller than the sums of the respective atomic radii of the elements (r_{Tb} = 1.78 Å, r_{Co} = 1.25 Å, r_C = 0.77 Å)[27]. A decrease of the interatomic distances is noted: the shortest Tb1-C1 contact shrinks by ~7.6 %, and Tb3-Co2, Tb1-Tb1 and Co2-C4 by ~1.6 %, ~4.5 % and ~12.4 %, respectively (for atom labeling see Fig. 2 and Tables S1† and S2†). The observed decrease of the interatomic distances is comparable with that reported for TbCoC[28] and Tb_2C.[29] The exceptions are the shortest Tb-C contact [*i.e.*, $d_{(Tb1-C1)}$ = 2.355(9) Å] which is almost equal to the sum of the atomic radii of the elements in the case of TbCoC [$d_{(Tb-C)}$ = 2.517 Å] and shortened by only ~3.4 % in the binary Tb_2C [$d_{(Tb-C)}$ = 2.463 Å], and the contraction of the Co-C distance which is ~9.0 % in TbCoC [$d_{(Co-C)}$ = 1.826 Å] compared to 12.4 % in $Tb_4Co_2C_3$ [$d_{(Co2-C4)}$ = 2.355(9) Å].

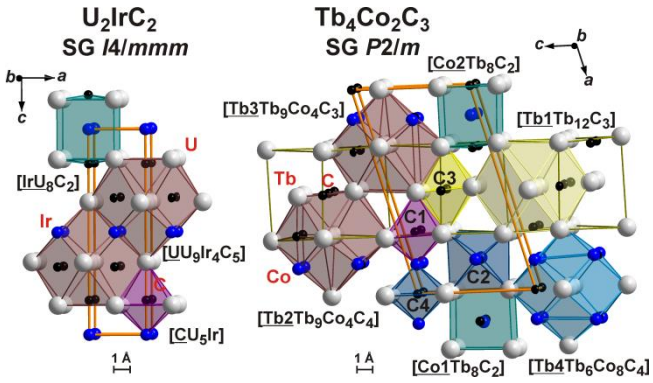

Fig. 2 Arrangements of the coordination polyhedra in the structures of the U_2IrC_2 (left) and $Tb_4Co_2C_3$ (right) types.

The coordination polyhedra in the structure of $Tb_4Co_2C_3$ are shown in Fig. 2. All Tb-atoms are centered at distorted cuboctahedra built of solely Tb atoms (*e.g.*, Tb1). Those with additional Tb-vertices occur in front of the faces formed by Co-atoms (*e.g.*, Tb2-Tb4). Interestingly, the carbon atoms lie nearly within the faces of the polyhedra without creating additional edges. As it can be seen in Fig. 2 a similar situation occurs for the cuboctahedra encountered in the structure of

Accepted manuscript

U_2IrC_2.[30] Additionally, in both $Tb_4Co_2C_3$ and U_2IrC_2 types *d*-elements adopt a cubic coordination with two C atoms lying in the opposite Tb_4/U_4 faces as well as an octahedral environment for carbon atoms. Interestingly, U_2IrC_2 is characterized by only one type of octahedra (*i.e.*, [CU_5Ir]), whereas in $Tb_4Co_2C_3$, besides analogous octahedral units [C1Tb_5Co], octahedra consisting either of solely Tb atoms (*i.e.*, [C3Tb_6]) or containing two Co vertices are observed, as in the case for C2 and C4 atoms.

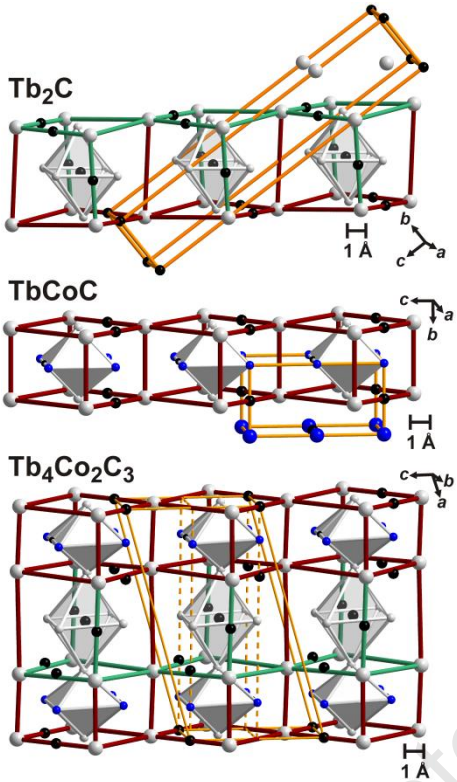

Fig. 3 Structural fragments in the related Tb_2C [SG $R\bar{3}m$, a = 3.584 Å, c = 18.04 Å][29] (top), TbCoC [SG $P4_2/mmc$, a = 3.6515 Å, c = 6.8651 Å][28] (middle), and $Tb_4Co_2C_3$ (bottom) structures. The unit cell for $Tb_4Co_2C_3$ reported earlier as "Tb_2CoC_2"[14] is indicated in dashed line.

The crystal structure of $Tb_4Co_2C_3$ is closely related with those of Tb_2C (anti-$CdCl_2$ type)[29] and TbCoC (YCoC type)[28] carbides (Fig. 3). The Tb_2C structure consists of distorted edge-sharing [Tb_8] cubes in which the 6 edges are centered by C atoms and wherein [CTb_6] octahedra are incorporated. Similar fragments (*i.e.*, [Tb_8] parallelepipeds with 4 Tb atoms centered by C atoms edges incorporating empty [□Co_4Tb_2] octahedra, where in the center of one edge a C atom is again located) occur in the TbCoC carbide. In conclusion, the $Tb_4Co_2C_3$ structure can be considered as an alternation of the above-mentioned fragments (Fig. 3).

Physical properties

Temperature dependent magnetic susceptibility $\chi(T)$ was measured for $Y_4Co_2C_3$, $Gd_4Co_2C_3$ and $Tb_4Co_2C_3$ in magnetic fields between 1 and 7 T in both field-cooling *(FC)* and zero-field-cooling *(ZFC)* cycles (Fig. 4). $\chi(T)$ of $Y_4Co_2C_3$ exhibits a weak field dependence at lower temperatures (inset in Fig. 4). This is attributed to minute amount of ferromagnetic impurities, the magnetization of which saturates with increasing magnetic fields. The weak temperature dependence in $\chi(T)$ of $Y_4Co_2C_3$ can be ascribed to ~0.2 % Gd atoms (spin S = 7/2) per formula unit (f.u.), consistent with the purity level (99.9%) of the Y metal ingots used for the syntheses. Extrapolating $\chi(T)$ to $T \rightarrow \infty$ ($\equiv 1/T \rightarrow 0$ in Fig. 4) and correcting by the diamagnetic increments[31], one obtains a Pauli susceptibility of +690 ± 20 $\times 10^{-6}$ emu mol^{-1} per f.u. for $Y_4Co_2C_3$. This indicates that the cobalt atoms are non-magnetic in the structure, similarly as it has been reported for YCoC.[32]

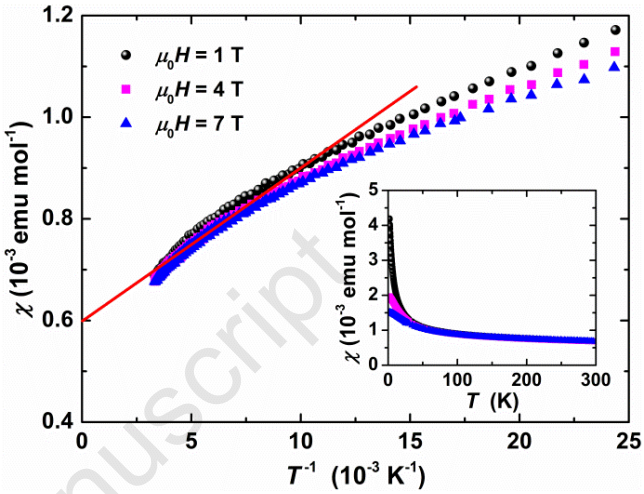

Fig. 4 Magnetic susceptibility of $Y_4Co_2C_3$ as a function of the inverse temperature measured in different fields as indicated. The solid red line is a fit to $\chi = C/T + \chi_0$, with C = 0.015 emu K mol^{-1}. Inset: magnetic susceptibility versus T.

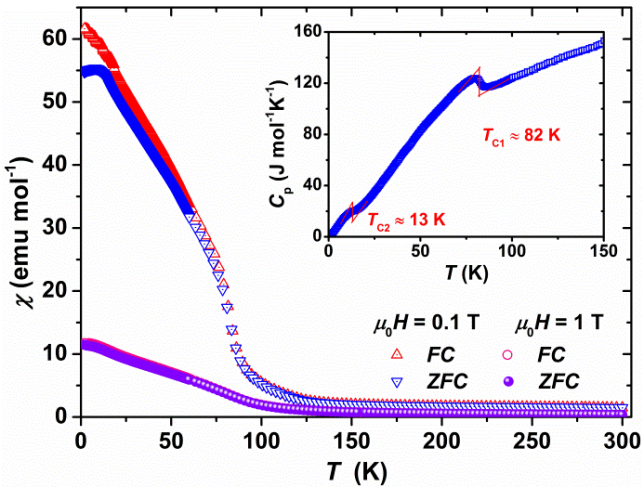

Fig. 5 Temperature dependence of the magnetic susceptibility of $Gd_4Co_2C_3$ measured in different fields and *ZFC* and *FC* regimes. Inset: specific heat of $Gd_4Co_2C_3$ (μ_0H = 0 T) together with the graphical equal area approximations (red lines) aiming the estimation of the transition temperatures

Temperature dependence of magnetic susceptibility and specific heat for $Gd_4Co_2C_3$ reveal two magnetic transitions at T_{C1} = 82(3) K and T_{C2} = 13(2) K (Fig. 5 and inset therein). The high temperature transition is preceded by a deviation of $\chi(T)$ from Curie-Weiss-like (*i.e.,* hyperbolic) dependence below ~150 K

Accepted manuscript

possibly due to short-range ordering. Additionally, $\chi(T)$ of $Gd_4Co_2C_3$ could be affected by Gd_2C and $GdCo_2$ impurities (Fig. S3†), which order ferromagnetically at T_C = 351 K[33] and T_C = 398 K,[34] respectively. This could explain the slight field dependence susceptibilities in the temperature range 200–300 K (see Fig. 5). The transition at ~82 K is ascribed to a long-range ferromagnetic ordering. As shown in Fig. S5† the magnetization of $Gd_4Co_2C_3$ displays typical ferromagnetic saturation behaviour with the low-temperature high-field moment approaching μ_{max} = 25.8 μ_B/f.u., which amounts to ~95 % of the full magnetic saturation for gadolinium.[35] A linear extrapolation of the M^2 *vs.* H/M curves (Arrott-Belov plots)[36] for $Gd_4Co_2C_3$ shown in Fig. 6, crosses the origin of the coordinate system for 80 K < T < 90 K, consistent with the high temperature transition found at T_{C1} = 82(3) K. A detailed plot of the curve parallel to the 80 and 90 K traces allows to estimate a value of 84(2) K in perfect agreement with $\chi(T)$ and $C_p(T)$ analysis. The nature of the second transition at ~13 K remains unclear at the present time but could tentatively be ascribed to re-ordering of the Gd moments. The field dependences of the magnetization measured at 2 K and 10 K, *i.e.*, below the transition at T_{C2} = 13(2) K, almost coincide. The remarkably large neutron absorption cross section of Gd nucleus hampers any further investigation of the exact nature of the arrangement of the magnetic moment in $Gd_4Co_2C_3$ by neutron diffraction.

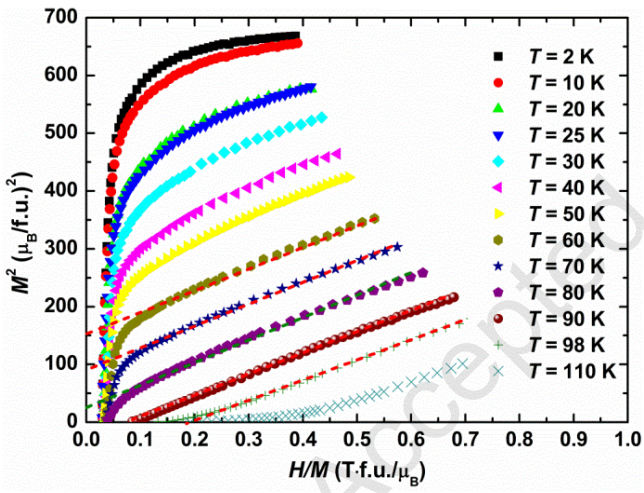

Fig. 6 Arrott-Belov plots for $Gd_4Co_2C_3$. The dashed lines are linear extrapolations.

The temperature dependence of the magnetic susceptibility of $Tb_4Co_2C_3$ is depicted in Fig. 7. Two magnetic transitions at T_C = 266 K (due to Tb_2C impurity phase)[37–39] and at T_C = 35(1) K corresponding to the targeted $Tb_4Co_2C_3$ compound are observed. The latter transition temperature is confirmed by measurements of the specific heat (inset in Fig. 7) as well as by Arrott-Belov plots (Fig. S6†). The ferromagnetic (or ferrimagnetic) nature of the ordering at T_C = 35(1) K is evidenced by the strong magneto-crystalline anisotropy (reflected in the significant change of $\chi(T)$ while performing measurements in *ZFC* and *FC* regimes[40]) as well as by the pronounced hysteresis observed in the isothermal magnetization loops (Fig. 8). So far, our attempts to refine the magnetic structure of $Tb_4Co_2C_3$ assuming a commensurate ferromagnetic phase from NPD pattern measured at 10 K, were not successful. Additional studies addressing this issue are in progress.

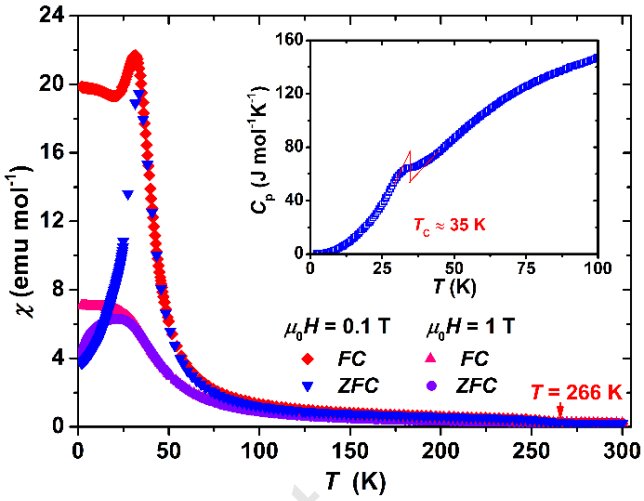

Fig. 7 Temperature dependence of the magnetic susceptibility of $Tb_4Co_2C_3$ measured in different fields and *ZFC* and *FC* regimes. Inset: specific heat of $Tb_4Co_2C_3$ (μ_0H = 0 T) together with the graphical equal area approximations (red lines) aiming the estimation of the transition temperatures.

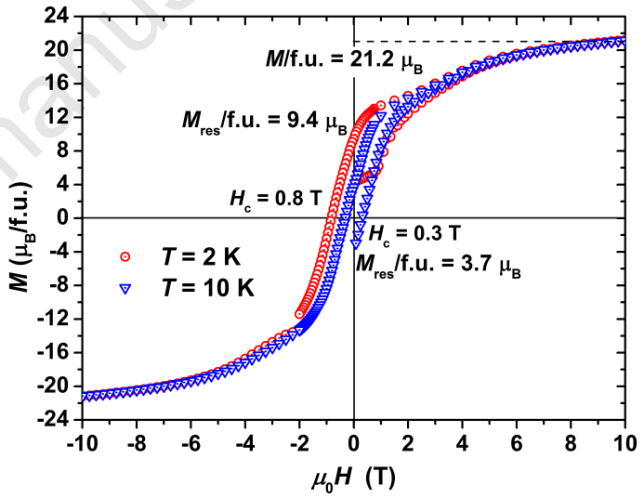

Fig. 8 Magnetic hystereses at low temperatures for $Tb_4Co_2C_3$.

In any case, the performed measurements indicate $Tb_4Co_2C_3$ to be a weak permanent magnet for T_C < 35 K with a remanence of 9.4 and 3.7 μ_B/f.u. The coercive field of μ_0H_c is ~0.8 and 0.3 T at 2 and 10 K, respectively (Fig. 8). The magnetization value at the highest reachable field of 10 T is μ_{max} = 21.2 μ_B/f.u., which is ~70 % of the full magnetic saturation for terbium.[41] Obviously, magnetic saturation in the $Tb_4Co_2C_3$ ferromagnet is not reached at 10 T, which is also clearly visible from the magnetization isotherms shown in Fig. 9. The difference to the theoretically expected magnetic moment of 9 μ_B/Tb-atom could be due to crystal electric field effects but also indicate strong pinning of the ferromagnetic domains.[42] Indeed, $M(H)$ curves of $Tb_4Co_2C_3$ measured at 2 K reveal an unusual stair-like behaviour (inset in Fig. 9) which has completely disappeared at 10 K (Fig. 9).

Accepted manuscript

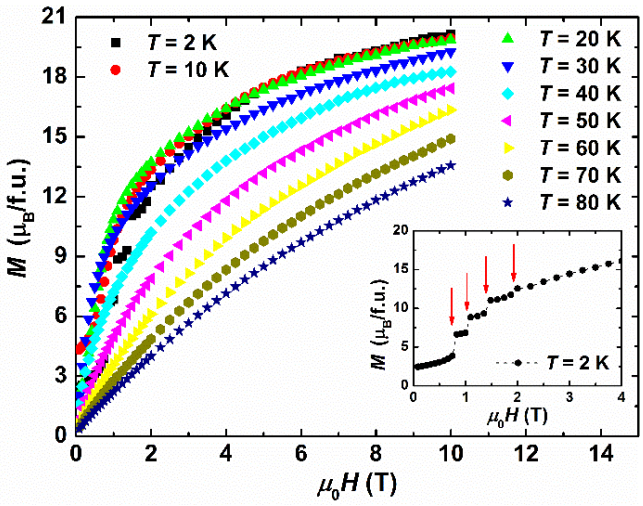

Fig. 9 Isothermal magnetization curves of $Tb_4Co_2C_3$. Inset: curve at 2 K, jumps in magnetization are indicated by red arrows.

Electronic structure and chemical bonding

The charge balanced formula for these rare earth transition metal carbides suggests a description of these phases as carbometalates with formal oxidation states as $(R^{3+})_4[(Co^0)_2(C^{4-})_3]$.[6] The computed total and atom-projected spin-polarized electronic DOS of $R_4Co_2C_3$ (R = Y, Gd, Tb) are sketched in Figs. 10–12. The DOS of all compounds reveal a rather high-energy dispersion, reflecting significant covalent interactions between cobalt and carbon atoms in particular, *i.e.*, in the complex anionic sublattice $[Co_2C_3]^{12-}$. Interestingly, the majority of the *d*-orbital projected DOS of the rare-earth metals is found above the Fermi level, confirming their d^0 character and their formal 3+ oxidation state. For cobalt atoms, most of the *d*-orbital projected DOS are located below the Fermi level. This confirms that the formal oxidation state of the transition metal atoms is rather zero in these compounds. These findings are in agreement with the charge balanced formulation $(R^{3+})_4[(Co^0)_2(C^{4-})_3]$ proposed above. The presence of Co^0 in $R_4Co_2C_3$ contrasts, for example, with the partially oxidized cobalt atoms (Co^+) observed in YCoC.[43,44] In the case of $Y_4Co_2C_3$, spin-up and spin-down total and projected DOS are nearly identical (Fig. 10). This corroborates the magnetic properties of this compound, which confirm nonmagnetic cobalt atoms (see above). On the other hand, as expected, the DOS of $Gd_4Co_2C_3$ and $Tb_4Co_2C_3$ highlight the strong polarization of the unpaired 4*f* electrons of the Gd (Fig. 11) and Tb (Fig. 12) atoms. Spin polarization hardly affects the other atoms. For Gd, the spin-up *f*-orbital projected DOS is fully occupied whereas the spin-down one is empty, corresponding to a $4f^7$ electronic configuration. For Tb, the spin-up *f*-orbital projected DOS is also fully occupied and the spin-down *f*-orbital projected DOS is slightly partially occupied. This corresponds to a $4f^8$ electronic configuration. Computed magnetic moments confirm that the magnetization resides almost entirely on the rare earth metal sites, and that they are responsible of the magnetic properties of the $R_4Co_2C_3$ phases since that of Co vanishes in the three compounds – indeed, a very weak polarization induced by the magnetism of R is computed (μ_B (Co) = 0.18 and 0.12 with Gd and Tb, respectively) – whereas those of Gd and Tb are 6.85 μ_B (spin component μ_{spin} = 6.82 μ_B and orbital component μ_{orb} = 0.03 μ_B) and 7.31 μ_B (μ_{spin} = 5.76 μ_B and μ_{orb} = 1.55 μ_B), respectively. These values or, more specifically, the trend from the calculated magnetic moments is consistent with the experimental magnetic data that were discussed above. Finally, metallic character is expected for all compounds with the Fermi level crossing substantial peaks of DOS.

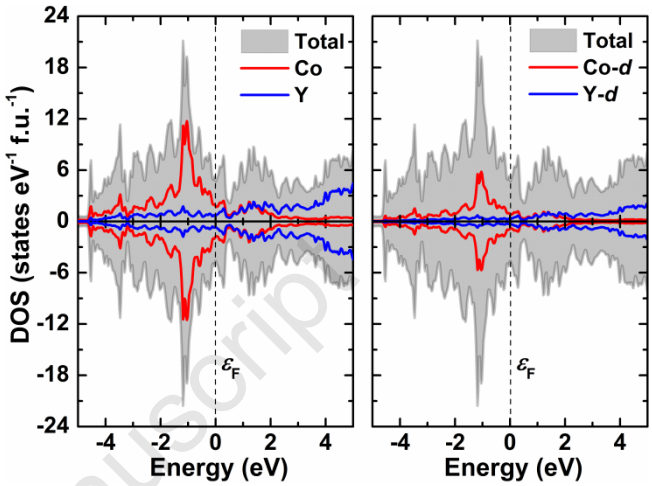

Fig. 10 Total, atom- and orbital-projected spin-polarized DOS of $Y_4Co_2C_3$. The dashed lines indicate the Fermi level (ε_F).

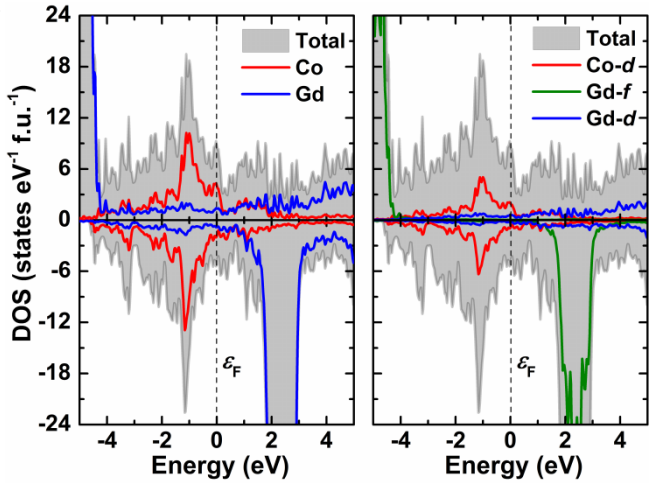

Fig. 11 Total, atom- and orbital-projected spin-polarized DOS of $Gd_4Co_2C_3$. The dashed lines indicate the Fermi level (ε_F).

Accepted manuscript

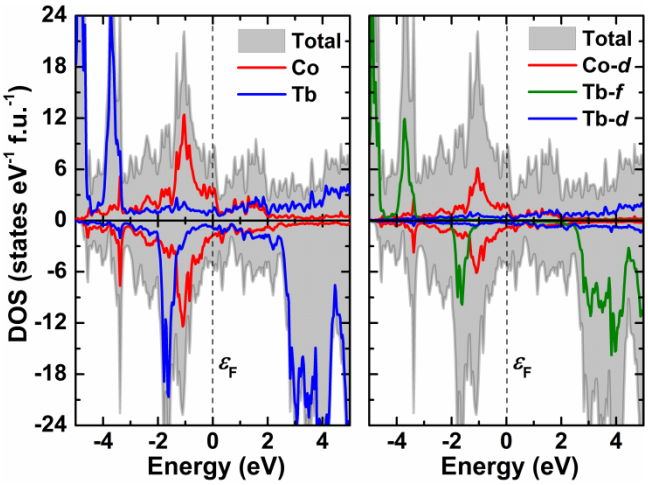

Fig. 12 Total, atom- and orbital-projected spin-polarized DOS of $Tb_4Co_2C_3$. The dashed lines indicate the Fermi level (ε_F).

Conclusions

A series of new ternary carbometalates $R_4Co_2C_3$ (R = Y, Gd, Tb) were synthesized and their crystal structure, electronic and magnetic properties were investigated. The crystal structure of $Tb_4Co_2C_3$ was refined from the neutron powder diffraction data collected at 100 K. Based on the powder X-ray diffraction experiment the phases $R_4Co_2C_3$ (R = Y, Gd) were found to show the same structural arrangement. $Tb_4Co_2C_3$ crystallizes with a unique structure-type among the ternary carbides, which consists of the stacking of alternating fragments observed in the Tb_2C (an anti-$CdCl_2$) and TbCoC (YCoC type) structures.

Temperature and field dependent magnetic susceptibility and magnetization measurements revealed $Y_4Co_2C_3$ to be a Pauli-paramagnet, whereas $Gd_4Co_2C_3$ orders ferromagnetically at T_{C1} = 82(3) K. The anomaly in the heat capacity at T_{C2} = 13(2) K was tentatively ascribed to a second magnetic transition, possibly due to re-ordering of the Gd moments. $Tb_4Co_2C_3$ orders ferromagnetically at T_C = 35(1) K. Electronic structure calculations confirmed that the magnetic moments are exclusively due to the rare-earth elements and that a charge-balanced situation can be formulated as $(R^{3+})_4[(Co^0)_2(C^{4-})_3]$, suggesting that the $R_4Co_2C_3$ compounds belong to the group of the carbometalates.

Author Contributions

V. Levytskyi: investigation, conceptualization, methodology, software, visualization, and writing-original draft. O. Isnard, R. K. Kremer, V. Babizhetskyy, B. Fontaine, X. Rocquefelte, J.-F. Halet: investigation, software, writing-reviewing and editing. R. Gumeniuk: formal analysis, visualization, writing-reviewing and editing.

Conflicts of interest

There are no conflicts to declare.

Acknowledgements

Authors are thankful to CNRS-CRG team at ILL for NPD data collection. VL acknowledges the support from the University Grenoble Alpes (France). We are also grateful to B. Ya. Kotur for his steady interest in this work.

References

1 J. Wang and Y. Zhou, *Annu. Rev. Mater. Res.*, 2009, **39**, 415–443.
2 Silicon Carbide. Volume 2: Power Devices and Sensors, ed. P. Friedrichs, T. Kimoto, L. Ley and G. Pensl, Wiley-VCH Verlag GmbH & Co. KGaA - Weinheim, 1st ed., 2009, 520 p.
3 J. H. Westbrook, *Metall. Trans. A*, 1977, **8A**, 1327–1360.
4 F. A. Cotton, G. Wilkinson, C. A. Murillo, and M. Bochmann, Advanced Inorganic Chemistry, John Wiley and Sons, New York, 6th ed., 1999, 1376 p.
5 E. Dashjav, F. R. Wagner, G. Kreiner, W. Jeitschko, and R. Kniep, *J. Solid State Chem.*, 2007, **180**, 636–653.
6 V. Babizhetskyy, B. Kotur, V. Levytskyy and H. Michor, in *Handbook on the Physics and Chemistry of Rare Earths Including Actinides*, ed. J.-C. G. Bünzli and V. K. Pecharsky, North-Holland, Amsterdam, 2017, 52, pp. 1–263.
7 G. Block and W. Jeitschko, *J. Solid State Chem.*, 1987, **70**, 271–280.
8 M. W. Dirken, R. C. Thiel, T. H. Jacobs, and K. H. J. Buschow, *J. Less-Common Met.*, 1991, **168**, 269–276.
9 R. Pöttgen, W. Jeitschko, C. Evers, and M. A. Moss, *J. Alloys Compd.*, 1992, **186**, 223–232.
10 P. Villars and K. Cenzual, Pearson's Crystal Data: Crystal Structure Database for Inorganic Compounds, 2010.
11 U. E. Musanke, W. Jeitschko, and M. E. Danebrock, *Z. Anorg. Allg. Chem.*, 1993, **619**, 321–326.
12 U. A. Böcker, W. Jeischko, and G. Block, *J. Alloys Compd.*, 1996, **236**, 58–62.
13 R. Pöttgen, K. H. Wachtmann, W. Jeitschko, A. Lang, and T. Ebel, *Z. Naturforsch.*, 1997, **52b**, 231–236.
14 V. Levytskyy, V. Babizhetskyy, and B. Kotur, in *Coll. Abstracts of XIII International Conference on Crystal Chemistry of Intermetallic Compounds*, Lviv, Ukraine, 25–29 September 2016, p. 76.
15 *STOE WinXPow* (ver. 2.10), Stoe & Cie GmbH, Darmstadt, Germany, 2004.
16 L. Akselrud and Y. Grin, *J. Appl. Crystallogr.*, 2014, **47**, 803–805.
17 A. Altomare, C. Cuocci, C. Giacovazzo, A. Moliterni, R. Rizzi, N. Corriero, and A. Falcicchio, *J. Appl. Crystallogr.*, 2013, **46**, 1231–1235.
18 I. Puente Orench, J. F. Clergeau, S. Martínez, M. Olmos, O. Fabelo, and J. Campo, *J. Phys.: Conf. Ser.*, 2014, **549**, 012003.
19 T. Roisnel and J. Rodriguez-Carvajal, *Mater. Sci. Forum*, *Proc. Seventh Eur. Powd. Diffr. Conf.* (EPDIC 7), 2000, p. 118–123.
20 J. Rodríguez-Carvajal, *Comm. Powd. Diffr. (IUCr). Newsletter*, 2001, **26**, 12–19.
21 A. Barlet, J. C. Genna, and P. Lethuillier, *Cryogenics*, 1991, **31**, 801–805.
22 K. Schwarz, P. Blaha and G. K. H. Madsen, *Comput. Phys. Commun.*, 2002, **147**, 71–76.
23 P. Blaha, K. Schwarz, G. Madsen, D. Kvasnicka, and J. Luitz, *WIEN2K: An Augmented Plane Wave + Local Orbitals Program for Calculating Crystal Properties*, TU Wien, Austria, 2001.
24 J. P. Perdew, K. Burke, and M. Ernzerhof, *Phys. Rev. Lett.*, 1996, **77**, 3865–3868.
25 F. Tran, P. Blaha, K. Schwarz, and P. Novák, *Phys. Rev. B*, 2006, **74**, 155108.

Accepted manuscript

26 R. A. Susilo, X. Rocquefelte, J. M. Cadogan, E. Bruyer, W. Lafargue-Dit-Hauret, W. D. Hutchison, M. Avdeev, D. H. Ryan, T. Namiki, and S. J. Campbell, *Phys. Rev. B*, 2019, **99**, 184426.
27 J. Emsley, The Elements, Oxford University Press, New York, 1998, 292 p.
28 M. H. Gerss and W. Jeitschko, *Z. Naturforsch.*, 1986, **41b**, 946–950.
29 M. Atoji, *J. Chem. Phys.*, 1981, **75**, 1434–1441.
30 H. Holleck, *J. Nucl. Mater*., 1968, **28**, 339–340.
31 P. W. Selwood, Magnetochemistry, Interscience Publ., New York, 2nd ed., 1956, 435 p.
32 M. E. Danebrock, W. Jeitschko, A. M. Witte, and R. Pöttgen, *J. Phys. Chem. Solids*, 1995, **56**, 807–811.
33 Y. Mudryk, D. Paudyal, V. K. Pecharsky, and K. A. Gschneidner, Jr., *J. Appl. Phys*., 2011, **109**, 07A924.
34 S. Khmelevskyi and P. Mohn, *J. Phys*.: *Cond. Matter*, 2000, **12**, 9453–9464.
35 J. F. Elliott, S. Legvold, and F. H. Spedding, *Phys. Rev.*, 1953, **91**, 28–30.
36 A. Arrott, *Phys. Rev.*, 1957, **108**, 1394–1396.
37 M. Atoji, *J. Chem. Phys.*, 1969, **51,** 3872–3876.
38 M. Atoji, *J. Chem. Phys.*, 1981, **75**, 1434–1441.
39 X. Zhang, S. Matsuishi, and H. Hosono, *J. Phys. D: Appl. Phys.*, 2016, **49**, 335002.
40 A. Menovsky, F. de Boer, P. Frings and J. France, in *High Field Magnetism*, ed. M. Date, North-Holland, Amsterdam, 1983, pp. 189–191.
41 W. E. Henry, *J. Appl. Phys.*, 1959, **30**, 99S-100S.
42 Q. Li, X. Yuan, L. Xing and M. Xu, *Sci. Rep.*, 2016, **6**, 27712.
43 R. Hoffmann, J. Li, and R. A. Wheeler, *J. Amer. Chem. Soc.*, 1987, **109**, 6600–6602.
44 D. J. Singh, *Phys. Rev. B*, 2002, **66**, 132414.

Accepted manuscript